

TaylorImNet for Fast 3D Shape Reconstruction Based on Implicit Surface Function

Yuting Xiao^{1*} Jiale Xu^{1*} Shenghua Gao^{1,2†}

¹ShanghaiTech University

²Shanghai Engineering Research Center of Intelligent Vision and Imaging

{xiaoyt, xujl1, gaosh}@shanghaitech.edu.cn

Abstract

Benefiting from the contiguous representation ability, deep implicit functions can extract the iso-surface of a shape at arbitrary resolution. However, utilizing the neural network with a large number of parameters as the implicit function prevents the generation speed of high-resolution topology because it needs to forward a large number of query points into the network. In this work, we propose TaylorImNet inspired by the Taylor series for implicit 3D shape representation. TaylorImNet exploits a set of discrete expansion points and corresponding Taylor series to model a contiguous implicit shape field. After the expansion points and corresponding coefficients are obtained, our model only needs to calculate the Taylor series to evaluate each point and the number of expansion points is independent of the generating resolution. Based on this representation, our TaylorImNet can achieve a significantly faster generation speed than other baselines. We evaluate our approach on reconstruction tasks from various types of input, and the experimental results demonstrate that our approach can get slightly better performance than existing state-of-the-art baselines while improving the inference speed with a large margin. Our code will be released in <https://github.com/svip-lab/TaylorImNet>.

1. Introduction

Deep implicit functions parameterized by neural networks have gained much popularity in 3D shape reconstruction and representation. Compared with explicit shape representations such as voxels [14, 17, 38], point clouds [1, 30, 31, 41] and meshes [22, 37], deep implicit functions represent the shape surface as the continuous decision boundary. At the inference phase, deep implicit functions predict the occupancy or signed distance field (SDF) for

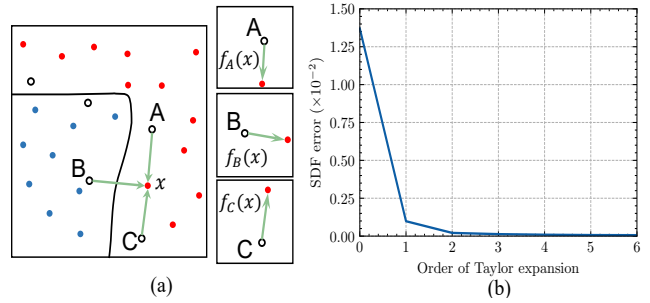


Figure 1. (a) The illustration of our Taylor implicit functions. We represent a shape with a set of expansion points (Hollow Black) and corresponding Taylor series. Each expansion point controls a local region around it. The signed distance of a query point x is computed by the weighted average of the Taylor series at the nearby expansion points A, B and C . (b) The evaluation of the representation capacity of the Taylor series. We separately sample 1000 expansion points from 1300 objects in the ShapeNet dataset and apply the least-squares method to estimate the Taylor series coefficients of each expansion point. We visualize the mean error of SDF estimated by different-order Taylor series, the results demonstrate that low-order Taylor series can already represent the shape accurately.

each querying position and extract the iso-surface with a post-processing step, *i.e.*, marching cubes [24]. The implicit functions separate each point in the space into inside and outside and can generate a continuous iso-surface for each shape. Some previous works [6, 25, 33] apply neural network as the implicit function to generalize all shapes, while some other works [13, 19] observe that the global 3D implicit representation may be hard to model and generalize because the possible global shapes are too diverse and might be too complex. So these works attempt to use the deep network to infer the local 3D representation because the local appearances of different objects are similar and easy to generalize.

However, deep implicit functions need to forward the neural network for every query point at the inference phase,

*Equal contribution.

†Corresponding author.

which is computation-unfriendly when generating surface at high resolution since there will be a large amount of points to query. Enhancing the capacity of the neural network to model complex shapes inevitably leads to increasing computational requirements and it is difficult to balance the capacity demand of the neural network and inference speed. Besides, though some works have discussed using a deep network with a large capacity to infer the parameters of a simple network for modeling the local region, which is similar to the conditional convolution, it is still tough to apply these approaches in reconstruction because the redundancy of parameters makes the parameter prediction too difficult, even it is a very simple deep network.

In this paper, inspired by the Taylor expansion, we propose a Taylor-series-based compact implicit local 3D shape representation to solve the aforementioned problem. Each object is represented by an expansion point set and the corresponding Taylor series. Furthermore, we propose a coarse-to-fine expansion points sampling strategy in the inference phase. The number of expansion points is independent of the resolution of mesh generation. Instead of utilizing the neural network to evaluate every query point, adopting the discrete point set and corresponding Taylor series to represent 3D shapes makes the inference independent to the neural network once the expansion points and corresponding coefficients are obtained. This representation can also take advantage of the learning ability of the neural network meanwhile promoting the computational efficiency when generating high-resolution topology since the time of inferring the coefficients of the Taylor series is fixed for each object and it does not need to forward the network for new query points.

Applying a single expansion point to cover a local region makes the global shape field discrete. To model the contiguous surface, we compute the weighted average of the Taylor series among several nearest expansion points of each query point, as shown in Figure 1 (a). The union of local regions around every expansion point can cover the global shape region. After the expansion points and the corresponding Taylor series coefficients are obtained, we can infer the signed distance field of arbitrary points in the space.

We evaluate our approach on the 3D object reconstruction task with 3 different input types: single-view images, point clouds, and voxels. In our experiments, we observe that only applying low-order Taylor series can reconstruct shape accurately, which is consistent with the experimental results in Figure 1 (b). And the inference speed is improved with a large margin compared with classical implicit function-based baselines.

The contributions of this paper could be summarized as:

- We propose a compact and computational-friendly implicit 3D shape representation based on the Taylor expansion.

- We propose a coarse-to-fine expansion points sampling strategy in the inference phase. This process is independent of the resolution of mesh generation.
- We demonstrate our implicit 3D representation can significantly speed up the generation while generating meshes with slightly better quality than existing state-of-the-art baselines on different input data types.

2. Related Work

3D Shape Reconstruction. There has been significant work on 3D shape reconstruction from various types of shape observations. Given a single-view image, 3D-R2N2 [8], PSGN [11], AtlasNet [16], Pixel2Mesh [37] and Pix2Vox [39] can reconstruct an explicitly represented model, *e.g.*, voxel grids, point clouds and meshes. Compared to explicit shape representations, implicit functions parameterized by neural networks is more memory-efficient and can preserve fine-grained shape details, thus they are adopted by many methods, *e.g.*, OccNet [25], and PIFu [33]. Different from single-view reconstruction which is an ill-posed problem, reconstruction from discrete point clouds or coarse voxel grids leads to finer shapes due to the 3D prior knowledge provided by them inherently. Given a point cloud as input, traditional optimization-based methods such as Moving Least Square [2] and Poisson Surface Reconstruction [20, 21], and deep optimization-based methods such as SAL [3] and IGR [15], can generate a continuous surface with fine details. When ground truth point-occupancy pairs are available, implicit-function-based methods such as OccNet [25] and ConvOccNet [29] can also address this task well. Besides, these implicit-function-based models [7, 25, 29] can also reconstruct high-resolution surfaces from coarse voxel grids (*i.e.*, voxel super-resolution) by assembling a proper 3D convolutional encoder. Despite the preferable performance, implicit-function-based methods need a post-processing step (*e.g.*, Marching Cubes [24]) to extract the iso-surface, which is often time-consuming at high resolution.

Global Shape Representations. Global shape representations seek to represent a 3D shape with a single implicit latent code. Following this spirit, an auto-encoder (AE) architecture is often exploited [6, 25]. Specifically, an encoder maps the input shape observation into the latent space, and a decoder tries to recover the shape with the holistic latent code. In comparison, DeepSDF [27] adopts an auto-decoder scheme, which randomly samples a latent code from a Gaussian prior distribution for each shape and optimizes it with gradient descent during the training process. A series of work [9, 10, 26, 34, 42] has made improvements upon the framework of DeepSDF and has shown promising shape modeling results. Global shape representations have good shape completion ability and the learned latent space

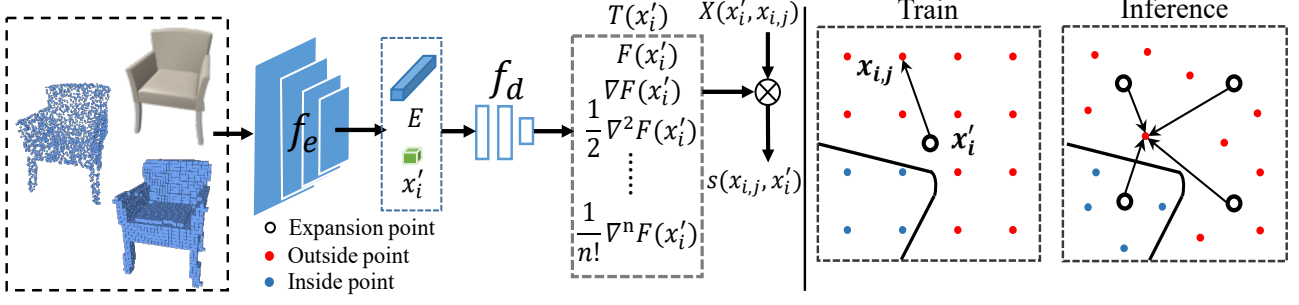


Figure 2. The Overview of our model. The input data types of this framework can be the single-view, the point cloud, or the voxel. In the training phase, Each expansion point x'_i has a set of sampled points nearby and the signed distance of each point $x_{i,j}$ in this set is computed based on the implicit Taylor series at expansion point x'_i . In the inference phase, after the expansion points sampling, the signed distance of arbitrary point x are inferred by the weighted average of the implicit Taylor expansion functions corresponding to its multiple nearest expansion points.

is convenient for shape interpolation and generation. However, they struggle to recover fine details. Thus, some recent work [35, 36] seek to use periodic activation functions for better preserving high-frequency details.

Local Shape Representations. Local shape representations decompose a holistic shape into local parts to better preserve fine details. Some methods learn to decompose the shape into local parts automatically, and represent the parts with CSG primitives [32], superquadrics [28] or 3D Gaussians [12, 13]. Dualsdf [18] expresses shapes at two levels of granularity, one capturing fine details and the other representing an abstracted proxy shape. Another set of work seeks to divide the 3D space into local patches. DeepLS [4] uniformly divides the 3D space into voxel grids and assigns a latent code as well as a DeepSDF decoder to each voxel. LGCL [40] adopts a similar idea except that the space partition is defined by a set of key points. LIG [19] train a part auto-encoder to learn an embedding of local crops of 3D shapes, and then the decoder is utilized to optimize the latent code of local crops at inference time.

3. Method

In this section, we introduce the modeling of our Taylor-based implicit 3D shape representation, how to train our approach, and how to utilize our coarse-to-fine to sample expansion points in the inference.

The classical deep implicit function based reconstruction methods first learn a latent representation c from the input partial 3D observations (*e.g.*, images, point clouds, voxels, and SDF grids), and then utilize a neural network to predict O (the SDF or occupancy value) of a query point x from the latent representation. This can be denoted as:

$$O = f(x, c) \quad (1)$$

Since that the f need to forward once for every query point, it is computationally unfriendly to generate high-resolution

meshes.

Our approach aims to utilize a fixed set of expansion points and corresponding Taylor series to represent a 3D shape. After these are obtained, the inferring of points is independent of the network-based decoder and this significantly speeds up the generation speed, especially for the high-resolution mesh.

3.1. Taylor-based Implicit Function Formulation

Given an signed distance field $F(x)$ of a shape, where the $x \in \mathbb{R}^3$ is the point coordinate. Our target is to utilize the combination of the Taylor series to represent the approximation of the $F(x)$. Suppose that $x'_i \in \mathbb{R}^3$ is an expansion point. We apply the Taylor series at this expansion point x'_i to model the target shape $F(x)$ at the local region near x'_i . The 3D representation of local region near the expansion point x'_i is denoted as $F_s(x, x'_i)$:

$$T(x'_i) = (F(x'_i), \nabla_x F(x'_i), \frac{1}{2}\nabla_x^2 F(x'_i), \dots) \quad (2)$$

$$X(x, x'_i) = (1, x - x'_i, (x - x'_i)(x - x'_i)^T, \dots) \quad (3)$$

$$F_s(x, x'_i) = T(x'_i) \cdot X(x, x'_i) \quad (4)$$

where the $T(x'_i)$ is the coefficients of the Taylor series at expansion point x'_i .

For an arbitrary point x in the space, inferring the $F(x)$ from the single nearest expansion point would make the signed distance field discontinuous. To alleviate the discontinuities, the $F(x)$ can be defined by the weighted average of the signed distance functions corresponding to multiple expansion points. Suppose that there is a set of expansion points \mathcal{P} close to the point x in the space, the $F(x)$ can be noted as:

$$F(x) = \sum_{x'_i \in \mathcal{P}} \omega(\|x - x'_i\|, \theta) F_s(x, x'_i) \quad (5)$$

where the \mathcal{P} denotes the set of expansion points in the n nearest neighbourhood of point x , and the weight

function is set as the Softmin function: $\omega(d_i, \theta) = \exp(-\theta d_i) / \sum_i \exp(-\theta d_i)$, since the expansion point far from the query point x should obtain large weight decay. d_i is the distance from the point x to the nearby expansion point x'_i .

3.2. Training Phase

We utilize an encoder f_e and a decoder f_d to infer the parameters of our Taylor series based 3D shape representation.

We randomly sample N expansion points in the 3D volume of an object. For each expansion point x'_i sampled in the space, we input the corresponding feature code \mathbf{E} and the position of this expansion point to the decoder f_d , and the output is the parameters $T(x'_i)$ of our implicit shape representation, which is denoted as:

$$T(x'_i) = f_d(c, x'_i) \quad (6)$$

After the parameters of an expansion point x'_i are obtained, we can predict the signed distance of any point x nearby this expansion point:

$$s(x, x'_i) = T(x'_i) \cdot X(x, x'_i)^T \quad (7)$$

Reconstruction loss. Directly applying the signed distance field for supervising the learning of the network is not applicable because the signed distance error at the point far from the surface is not significant for reconstruction. Aiming to lead the network to focus on the reconstruction of the surface region, we apply a sigmoid transformation on the signed distance field:

$$\sigma(s) = \frac{1}{1 + e^{-\alpha s}} \quad (8)$$

where α is a hyper-parameter. After the transformation, the points far from the surface would have almost the same distance value, and the decline in diversity makes the prediction easier than before the transformation. Besides, applying the TSDF (Truncated Signed Distance Field) and binary occupancy field has the same effect but both of them suffer from the existence of the non-differentiable points, which needs high order of Taylor series to approximate.

To supervise the inferred Taylor series coefficients $T(x'_i)$, we sample a grid of points centered around the expansion point x'_i and generate the ground truth signed distance values of these points. Suppose the $x_{i,j} \in \mathbb{R}^3$ is the j -th point in the point set sampled in the cube of the i -th expansion point x'_i and M points are sampled in the cube for each expansion point. We design the reconstruction loss function in the training phase as:

$$\mathcal{L} = \frac{1}{NM} \sum_{i=0}^N \sum_{j=0}^M \mathcal{L}_{ce}(\sigma(s(x_{i,j}, x'_i)), \sigma(F(x_{i,j}))) \quad (9)$$

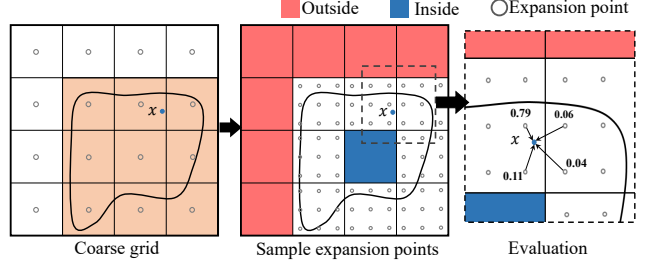


Figure 3. An example to introduce the coarse-to-fine strategy for expansion point sampling in the inference phase. A point is estimated by 4 nearest expansion points with the weights are 0.79, 0.11, 0.06, and 0.04 respectively.

where the N, M is the number of the expansion points and the sampled points in each group, and the \mathcal{L}_{ce} is the cross-entropy loss.

3.3. Inference Phase

In this section, we introduce the coarse-to-fine strategy to obtain the iso-surface of each object in the inference phase.

Firstly, a grid is generated to localize the coarse area of the surface. We divide the 3D volume with a low-resolution grid for sampling expansion points. For each unit of the grid, we sample the center point as the expansion point x'_i and compute the signed distance of this expansion point. An inside distance threshold ϵ_{in} and an outside threshold ϵ_{out} is set to filter the units into three classes: 1. outside units far from the surface; 2. inside unit far from the surface; 3. units near the surface. we aim to only sample dense expansion points in the units close to the surface, which can be denoted as:

$$\mathcal{R} = \{R(x'_i) | \epsilon_{in} \leq \sigma(s(x'_i, x'_i)) \leq \epsilon_{out}\} \quad (10)$$

where the $R(x'_i)$ is the region of the unit corresponding to the expansion point x'_i . The $s(x'_i, x'_i)$ can be consider as the Taylor expansion with 0 order at x'_i

Then, after the coarse surface regions are obtained, we sample more expansion points in each unit near the surface. This operation utilizes more expansion points to make the surface reconstruction more fine and smooth.

As shown in Figure 3. Based on the implicit 3D representation inferred by our model, we can infer the signed distance of arbitrary points in the space. For the point belonging to a unit far from the surface, the occupancy of this point is set to the same as the unit it belongs to. For the point belonging to the unit near the surface, we choose its k nearest neighborhood expansion points to compute the weighted average signed distance. The Marching Cubes algorithm to obtain the predicted iso-surface.

4. Experiments

In this section, we conduct experiments to validate the performance of our TaylorImNet. Firstly, we compare the reconstruction results on 3 different types of input quantitatively and qualitatively. Secondly, we demonstrate the inference acceleration effect compared with classical implicit-function-based methods. Thirdly, we conduct ablation studies to evaluate the representation capacity of our approach.

Dataset. Our experiments are conducted on the ShapeNet [5] dataset which contains 13 shape categories. We follow the data pre-processing operations in OccNet [25] for the fair comparison. For the single-view reconstruction and the voxel super-resolution task, we use the image renderings and model voxelizations provided by 3D-R2N2 [8]. For the point cloud reconstruction task, the point clouds sampled by [25] are exploited as input.

Metrics. Following the ConvOccNet [29], we quantify the performance of our method and other baselines with three metrics: (i) volumetric IoU (higher is better), (ii) Chamfer- L_1 distance (lower is better), and (iii) F-Score (higher is better). To compute the volumetric IoU, 100k points are uniformly sampled in the bounding volume of the mesh. The Chamfer- L_1 distance is computed by randomly sampling 100k points on the mesh surface and we scale the Chamfer- L_1 results by 10. The F-Score is reported with threshold $\tau = 0.01$.

Training Details. In the training phase, we sample 2 types of points: 1. expansion points for shape representation; 2. query points near each expansion point for supervising the prediction of Taylor series coefficients in Equation 9. For the expansion point sampling, we uniformly random sample k_1 expansion points in the bounding volume and k_2 expansion points near the surface. We set $k_1 : k_2 = 1 : 3$ in our implementation. For the query point sampling, we aim to sample a set of points near each expansion point. Treating a chosen expansion point as the center point, we evenly sample a 5^3 grid of query points in a cube whose side length equals 0.08. Based on this, each expansion point has 125 query points nearby. Besides, the α of the sigmoid transformation is set to 32. We use the Adam optimizer with $\beta_1 = 0.9$ and $\beta_2 = 0.999$. We train our model with a learning rate starting from 1×10^{-3} and divided by 10 for 2 times in the training. The implementation details of different data types are introduced in the supplementary material.

Inference Details. In the inference phase, take the single-view reconstruction as an example, our coarse-to-fine expansion point sampling strategy firstly samples a 16^3 grid of expansion points and we set $\epsilon_{out} = 0.98$ and $\epsilon_{in} = 0.02$ to filter the units near the surface. Then, we sample a 2^3 grid in each unit near the surface. After the expansion points are obtained, we apply the 4 nearest expansion points to evaluate the point in the unit near the surface.

	IoU \uparrow	Chamfer- L_1 \downarrow	F-Score \uparrow
3D-R2N2 [8]	0.500	0.246	0.347
PSGN [11]	-	0.215	0.142
Pixel2Mesh [37]	0.480	0.216	0.274
OccNet [25]	0.593	0.194	0.523
Ours	0.599	0.192	0.553

Table 1. The quantitative results of the single-view reconstruction task.

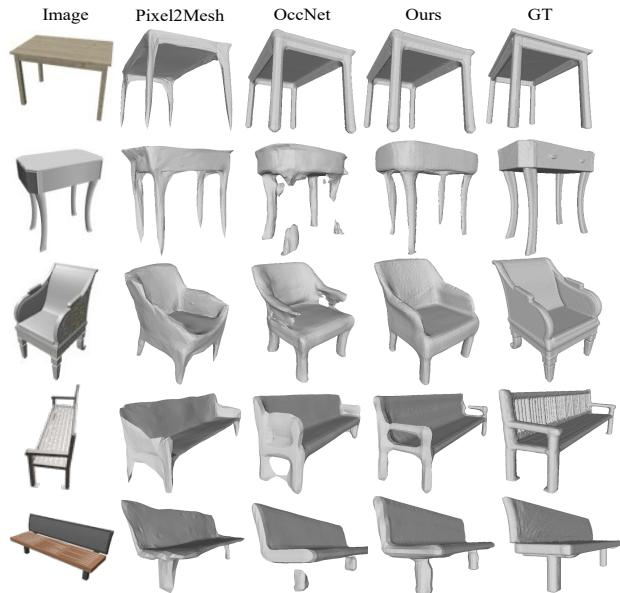


Figure 4. Qualitative results on single-view reconstruction task.

4.1. Reconstruction from Single-view Images

We first conduct the single-view reconstruction experiments. The image renderings provided by [8] are used as input, which contains 24 views for each shape. We compare our model with 4 baseline approaches: 3D-R2N2 [8], PSGN [11], Pixel2Mesh [37] and OccNet [25]. Our model uses the same backbone as OccNet and achieve slightly better performance, which indicates the efficient capacity of shape representation. The quantitative results are shown in Table 1. Our approach can obtain comparable performance on IoU and Chamfer- L_1 metrics.

We also show some qualitative results in Figure 4. We observe that our model achieves better performance on curved surface reconstruction than other compared baselines, such as the curved table legs and sleek chair armrests as shown in the 2nd and 3rd rows respectively. This benefited from the high-order terms of the Taylor series which can easily represent the curved surface compared with OccNet [25]. The pixel2mesh [37] can create sharp corners while hardly reconstructing smooth curved surfaces. And the table legs in the first row show that our approach can re-

	IoU \uparrow	Chamfer- L_1 \downarrow	F-Score \uparrow
PSGN [11]	-	0.178	0.180
DMC [23]	0.733	0.076	0.790
OccNet [25]	0.772	0.082	0.799
ConvOccNet [29]	0.870	0.048	0.933
Ours	0.875	0.043	0.945

Table 2. Quantitative comparison for point clouds reconstruction.

construct reasonable results on straight and sharp parts. The 4th and 5th rows show that our approach has enough ability to reconstruct the right angle area such as the right-angle handrail and pillar of chairs.

4.2. Reconstruction from Point Clouds

This task aims to reconstruct the mesh surface from a point cloud with noise. We randomly subsample 3000 points from point cloud provided by OccNet [25] as input and apply Gaussian noise with zero mean and standard deviation 0.005. The implementation of DMC [23] and PSGN [11] is adopted from the OccNet codebase¹. Our model uses the same backbone as ConvOccNet [29] with its volume encoder.

The quantitative results are shown in Figure 5. Our approach and ConvOccNet can obtain obviously more reasonable results than other baselines. And compared with ConvOccNet, our approach has a significant advantage for generating flat and narrow shape parts and holes. The red dotted boxes in the last 3 columns demonstrate that ConvOccNet can not reconstruct reasonable surfaces at the local region where the occupancy of points changes frequently. This situation happens when the different parts of a surface are stacked with each other. For example, the backplane of the tail of the airplane (1st row), the mezzanine under a chair cushion or the table (2nd, 4th, and 5th rows), and the region between the back of the display and the pillar (3rd row).

4.3. Voxel Super-Resolution

We also evaluate our method on the voxel super-resolution task, which takes coarse voxelizations (32^3) as input, and reconstruct meshes with high-resolution details. We use the same backbone as [29]. The quantitative results are shown in Table 3. Our method achieves better performance compared with other baselines.

It is noted that the coarse-to-fine expansion point strategy is simplified in the voxel super-resolution task as the units near the surface can be obtained from the voxel directly. For a unit of the input voxel, it is identified as a unit near the surface if the number of units near it is not 26 or 0. We observe that our approach can improve the performance comprehensively to other baselines.

¹https://github.com/autonomousvision/occupancy_networks

	IoU \uparrow	Chamfer- L_1 \downarrow	F-Score \uparrow
Input	0.631	0.136	0.440
OccNet [25]	0.703	0.110	0.656
ConvOccNet [29]	0.752	0.091	0.729
Ours	0.761	0.081	0.755

Table 3. Quantitative comparison for voxel super-resolution. The first row is the results of transforming the input voxels into meshes and computing the metrics directly.

4.4. Inference Speed

To demonstrate the inference speed promotion of our approach, we compare with OccNet [25] and ConvOccNet [29] on single-view and point cloud reconstruction. For our approach, once the expansion points are sampled and the corresponding Taylor series coefficients are predicted, the SDF value of arbitrary points can be computed with the Taylor series of nearby expansion points. In addition, the number of sampled expansion points from the coarse-to-fine strategy will not be influenced by the resolution of mesh generation. So, after the expansion points are obtained, the inference of our approach is independent of the deep neural network. In this section, we aim to statistic and analyze the inference speed on both the expansion sampling and the point evaluation.

We compare the inference speed of our approach with OccNet [25] and ConvOccNet [29] on mesh generation. The backbone of our approach on single-view and point cloud data types are the same as OccNet and ConvOccNet respectively. All the experiments in this section are implemented on one Titan V GPU. We only report the time spent on evaluating points. The time spent on marching cubes is not considered.

We can observe that, as the mesh resolution increases, the time increase of our approach is less significant than other baselines. As the mesh resolution increases, the time spent on other baselines increases about 4 to 8 times while our approach only increases by about 2 times. This is because our coarse-to-fine strategy for sampling expansion points is independent of the mesh resolution, the time on sampling expansion points would not increase with the mesh resolution increasing.

Besides, our approach spends more time on single-view reconstruction than point cloud reconstruction. The reason is that identifying the units near the surface is easier on point cloud data type. To guarantee the units which are identified near the surface can cover the surface as much as possible, the threshold ϵ_{in} and ϵ_{out} on single-view need to preserve a larger margin than point cloud. Based on this, the number of expansion points sampled in single-view reconstruction is often larger than point cloud reconstruction.

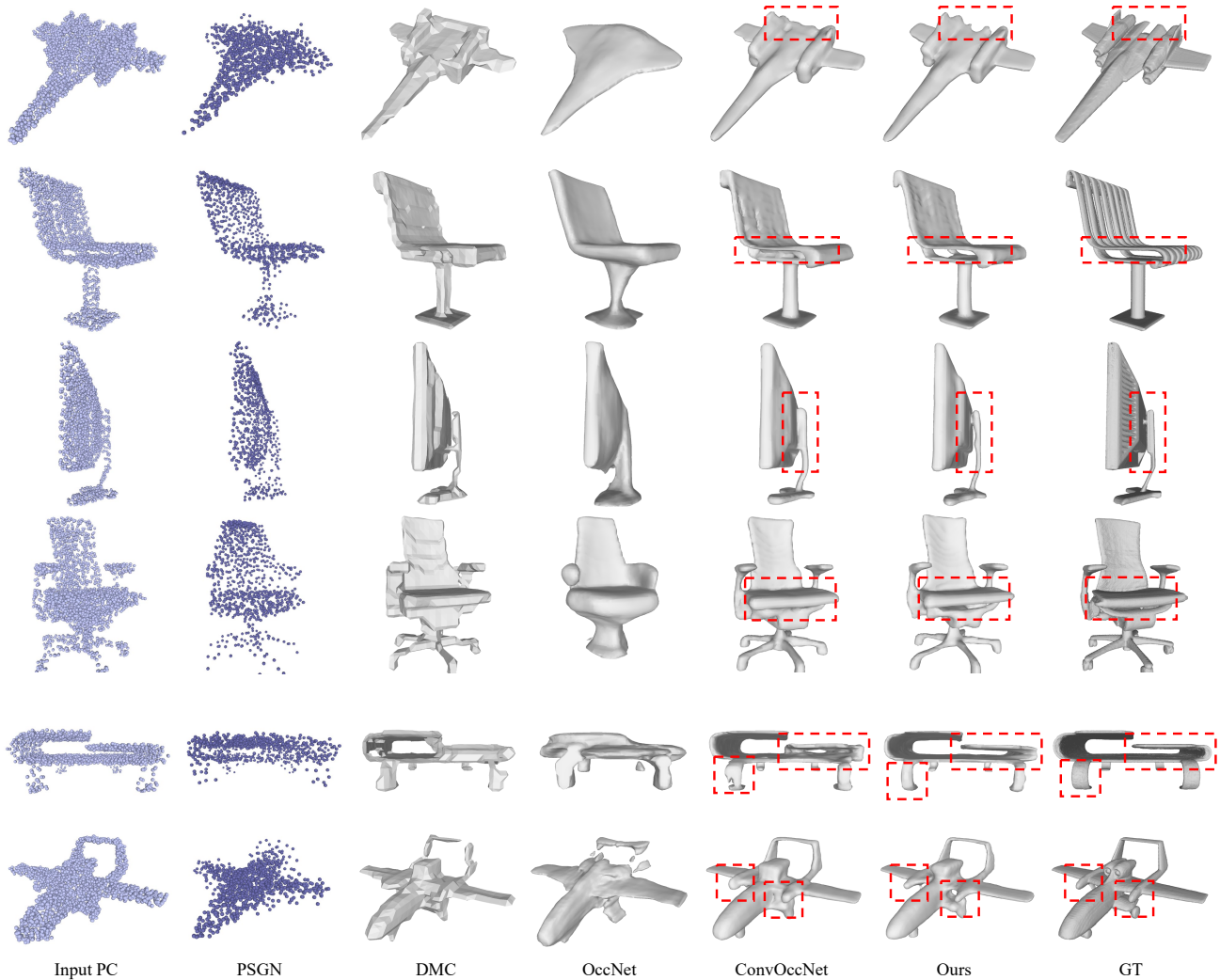


Figure 5. Qualitative results on point cloud reconstruction task. The red dotted boxes highlight the advantages of our approach.

Resolution	Single-view		Point cloud		
	OccNet	Ours	OccNet	ConvOccNet	Ours
64	0.101	0.031	0.171	0.113	0.024
128	0.783	0.069	0.916	0.492	0.035

Table 4. We statistic the average time spent (second) for each input sample in the point evaluation step.

4.5. Ablation Studies

In this section, we evaluate how the different orders of the Taylor series and different numbers of nearest expansion points in the inference affect the performance.

Order of Taylor Series To test the influence of the Taylor series with different orders, we visualize the generated meshes which are evaluated with coefficients of different

orders. For example, when we evaluate the results of the Taylor series with the order equal to 2, we only preserve the coefficients of terms with the order less than or equal to 2. The coefficients of Taylor series with the order larger than 2 are set to 0.

The qualitative results are shown in Figure 6. We observe that the terms with the order 0 and 1 of the Taylor series can provide a rough outline of the object while the terms with the higher order such as 2 and 3 represent the fine details of the object. Besides, this result also supports the aforementioned conclusion in Figure 1 (b), *i.e.*, the low-order Taylor series can provide an excellent shape approximation result. The improvement of increasing the order of the Taylor series from order 3 is too slight to be observed, which is also indicated by the quantitative results in Table 5.

Number of Nearest Expansion Points in Inference As

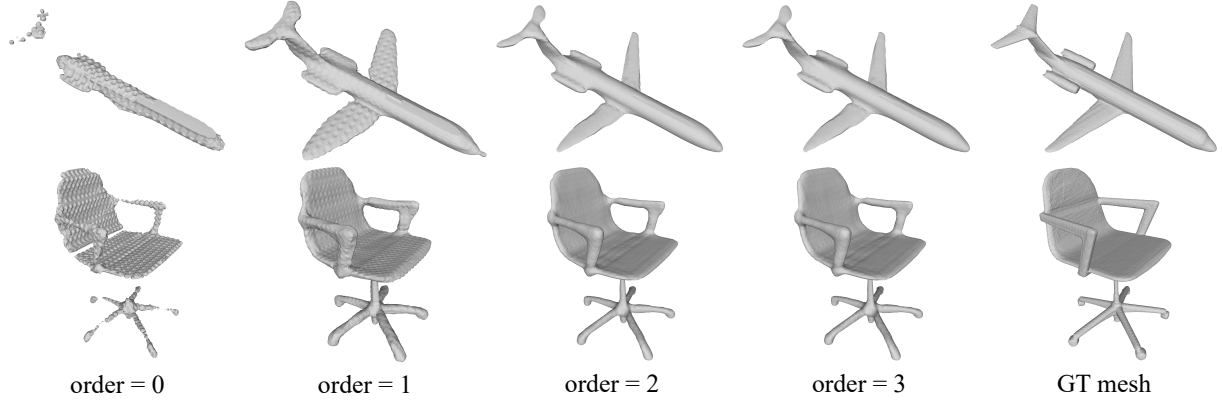


Figure 6. Qualitative results on point cloud reconstruction task with different Taylor series orders. Adopting Taylor series of order 2 or 3 has achieved excellent reconstruction results compared with the ground truth mesh. We do not visualize the mesh generated with order 4 since it has almost no difference from order 3.

Order	IoU \uparrow	Chamfer- L_1 \downarrow	F-Score \uparrow
0	0.726	0.101	0.762
1	0.800	0.057	0.890
2	0.874	0.043	0.944
3	0.875	0.043	0.945
4	0.875	0.043	0.945

Table 5. The quantitative comparison of using different orders of Taylor series to reconstruct from point clouds.

k	Single-view			Point cloud		
	IoU \uparrow	Chamfer- L_1 \downarrow	F-Score \uparrow	IoU \uparrow	Chamfer- L_1 \downarrow	F-Score \uparrow
1	0.593	0.193	0.543	0.867	0.045	0.940
2	0.598	0.192	0.551	0.872	0.044	0.944
4	0.599	0.192	0.553	0.875	0.043	0.945
8	0.600	0.196	0.550	0.876	0.043	0.946

Table 6. The influence of the number of nearest expansion points.

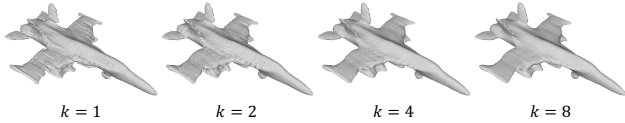


Figure 7. The visualization of the reconstruction results from a "plane" point cloud with varying numbers of expansion points at inference phase.

shown in Equation 5, we compute the weighted average of the Taylor series with k -nearest expansion points. To analyze how the value of k influences the performance, we set $k = 1, 2, 4, 8$ respectively in the inference phase, the results are shown in Table 6.

From the results, we can see that the weighted average operation among multiple expansion points promotes the performance significantly compared with using a single expansion point when $k \leq 4$. However, when $k > 4$, the performance degrades slightly because the expansion points far away the target query points provide less accurate prediction. Besides, exploiting larger k will lead to more memory usage. We empirically find $k = 4$ is a cost-effective setting and adopt it in all experiments.

To better demonstrate the influence of exploiting k -nearest expansion points, we visualize the reconstruction results of the "plane" point cloud with different values of k in Figure 7. It can be observed that by using a proper

number of expansion points and performing the weighted average, we can generate a smoother mesh and reduce the topology artifacts significantly.

5. Conclusion

In this work, we propose TaylorImNet, a compact implicit 3D shape representation based on the Taylor series for fast 3D shape reconstruction. In contrast to classical deep implicit functions, our Taylor-based implicit function is independent of the network in the inference phase, which significantly boosts the mesh generation speed than other baselines.

Our experiments on different input data types demonstrate that our TaylorImNet can not only speed up the mesh generation but also have comparable representation capacity compared with the existing state-of-the-art baselines. This proves the efficient representation capacity of our approach.

Broader Impact and Limitation Our experiments exploit the ShapeNet dataset which is publicly available, thus do not involve privacy issues. However, we did not test our approach on human datasets, thus cannot guarantee the generalization ability to model humans. Besides, TaylorImNet requires sampling a group of query points around each expansion point at the training phase, which leads to a larger amount of training query points than the baselines such as [25] and [29].

References

- [1] Panos Achlioptas, Olga Diamanti, Ioannis Mitliagkas, and Leonidas Guibas. Learning representations and generative models for 3d point clouds. In *International conference on machine learning*, pages 40–49. PMLR, 2018. 1
- [2] Marc Alexa, Johannes Behr, Daniel Cohen-Or, Shachar Fleishman, David Levin, and Claudio T. Silva. Computing and rendering point set surfaces. *IEEE Transactions on visualization and computer graphics*, 9(1):3–15, 2003. 2
- [3] Matan Atzmon and Yaron Lipman. Sal: Sign agnostic learning of shapes from raw data. In *Proceedings of the IEEE/CVF Conference on Computer Vision and Pattern Recognition (CVPR)*, June 2020. 2
- [4] Rohan Chhabra, Jan E Lenssen, Eddy Ilg, Tanner Schmidt, Julian Straub, Steven Lovegrove, and Richard Newcombe. Deep local shapes: Learning local sdf priors for detailed 3d reconstruction. In *European Conference on Computer Vision*, pages 608–625. Springer, 2020. 3
- [5] Angel X Chang, Thomas Funkhouser, Leonidas Guibas, Pat Hanrahan, Qixing Huang, Zimo Li, Silvio Savarese, Manolis Savva, Shuran Song, Hao Su, et al. Shapenet: An information-rich 3d model repository. *arXiv preprint arXiv:1512.03012*, 2015. 5
- [6] Zhiqin Chen and Hao Zhang. Learning implicit fields for generative shape modeling. In *Proceedings of the IEEE/CVF Conference on Computer Vision and Pattern Recognition*, pages 5939–5948, 2019. 1, 2
- [7] Julian Chibane, Thiemo Alldieck, and Gerard Pons-Moll. Implicit functions in feature space for 3d shape reconstruction and completion. In *Proceedings of the IEEE/CVF Conference on Computer Vision and Pattern Recognition*, pages 6970–6981, 2020. 2
- [8] Christopher B Choy, Danfei Xu, JunYoung Gwak, Kevin Chen, and Silvio Savarese. 3d-r2n2: A unified approach for single and multi-view 3d object reconstruction. In *European conference on computer vision*, pages 628–644. Springer, 2016. 2, 5
- [9] Yu Deng, Jiaolong Yang, and Xin Tong. Deformed implicit field: Modeling 3d shapes with learned dense correspondence. In *Proceedings of the IEEE/CVF Conference on Computer Vision and Pattern Recognition*, pages 10286–10296, 2021. 2
- [10] Yueqi Duan, Haidong Zhu, He Wang, Li Yi, Ram Nevatia, and Leonidas J Guibas. Curriculum deepsdf. In *European Conference on Computer Vision*, pages 51–67. Springer, 2020. 2
- [11] Haoqiang Fan, Hao Su, and Leonidas J Guibas. A point set generation network for 3d object reconstruction from a single image. In *Proceedings of the IEEE conference on computer vision and pattern recognition*, pages 605–613, 2017. 2, 5, 6
- [12] Kyle Genova, Forrester Cole, Avneesh Sud, Aaron Sarna, and Thomas Funkhouser. Local deep implicit functions for 3d shape. In *Proceedings of the IEEE/CVF Conference on Computer Vision and Pattern Recognition*, pages 4857–4866, 2020. 3
- [13] Kyle Genova, Forrester Cole, Daniel Vlasic, Aaron Sarna, William T Freeman, and Thomas Funkhouser. Learning shape templates with structured implicit functions. In *Proceedings of the IEEE/CVF International Conference on Computer Vision*, pages 7154–7164, 2019. 1, 3
- [14] Rohit Girdhar, David F Fouhey, Mikel Rodriguez, and Abhinav Gupta. Learning a predictable and generative vector representation for objects. In *European Conference on Computer Vision*, pages 484–499. Springer, 2016. 1
- [15] Amos Gropp, Lior Yariv, Niv Haim, Matan Atzmon, and Yaron Lipman. Implicit geometric regularization for learning shapes. *arXiv preprint arXiv:2002.10099*, 2020. 2
- [16] Thibault Groueix, Matthew Fisher, Vladimir G Kim, Bryan C Russell, and Mathieu Aubry. A papier-mâché approach to learning 3d surface generation. In *Proceedings of the IEEE conference on computer vision and pattern recognition*, pages 216–224, 2018. 2
- [17] Christian Häne, Shubham Tulsiani, and Jitendra Malik. Hierarchical surface prediction for 3d object reconstruction. In *2017 International Conference on 3D Vision (3DV)*, pages 412–420. IEEE, 2017. 1
- [18] Zekun Hao, Hadar Averbuch-Elor, Noah Snively, and Serge Belongie. Dualsdf: Semantic shape manipulation using a two-level representation. In *Proceedings of the IEEE/CVF Conference on Computer Vision and Pattern Recognition*, pages 7631–7641, 2020. 3
- [19] Chiyu Jiang, Avneesh Sud, Ameesh Makadia, Jingwei Huang, Matthias Nießner, Thomas Funkhouser, et al. Local implicit grid representations for 3d scenes. In *Proceedings of the IEEE/CVF Conference on Computer Vision and Pattern Recognition*, pages 6001–6010, 2020. 1, 3
- [20] Michael Kazhdan, Matthew Bolitho, and Hugues Hoppe. Poisson surface reconstruction. In *Proceedings of the fourth Eurographics symposium on Geometry processing*, volume 7, 2006. 2
- [21] Michael Kazhdan and Hugues Hoppe. Screened poisson surface reconstruction. *ACM Transactions on Graphics (ToG)*, 32(3):1–13, 2013. 2
- [22] Nikos Kolotouros, Georgios Pavlakos, and Kostas Daniilidis. Convolutional mesh regression for single-image human shape reconstruction. In *Proceedings of the IEEE/CVF Conference on Computer Vision and Pattern Recognition*, pages 4501–4510, 2019. 1
- [23] Yiyi Liao, Simon Donne, and Andreas Geiger. Deep marching cubes: Learning explicit surface representations. In *Proceedings of the IEEE Conference on Computer Vision and Pattern Recognition*, pages 2916–2925, 2018. 6
- [24] William E Lorensen and Harvey E Cline. Marching cubes: A high resolution 3d surface construction algorithm. *ACM siggraph computer graphics*, 21(4):163–169, 1987. 1, 2
- [25] Lars Mescheder, Michael Oechsle, Michael Niemeyer, Sebastian Nowozin, and Andreas Geiger. Occupancy networks: Learning 3d reconstruction in function space. In *Proceedings of the IEEE/CVF Conference on Computer Vision and Pattern Recognition*, pages 4460–4470, 2019. 1, 2, 5, 6, 8
- [26] Jiteng Mu, Weichao Qiu, Adam Kortylewski, Alan Yuille, Nuno Vasconcelos, and Xiaolong Wang. A-sdf: Learning disentangled signed distance functions for articulated shape representation. *arXiv preprint arXiv:2104.07645*, 2021. 2

- [27] Jeong Joon Park, Peter Florence, Julian Straub, Richard Newcombe, and Steven Lovegrove. Deepsdf: Learning continuous signed distance functions for shape representation. In *Proceedings of the IEEE/CVF Conference on Computer Vision and Pattern Recognition*, pages 165–174, 2019. [2](#)
- [28] Despoina Paschalidou, Ali Osman Ulusoy, and Andreas Geiger. Superquadrics revisited: Learning 3d shape parsing beyond cuboids. In *Proceedings of the IEEE/CVF Conference on Computer Vision and Pattern Recognition (CVPR)*, June 2019. [3](#)
- [29] Songyou Peng, Michael Niemeyer, Lars Mescheder, Marc Pollefeys, and Andreas Geiger. Convolutional occupancy networks. In *Computer Vision—ECCV 2020: 16th European Conference, Glasgow, UK, August 23–28, 2020, Proceedings, Part III 16*, pages 523–540. Springer, 2020. [2](#), [5](#), [6](#), [8](#)
- [30] Charles R Qi, Hao Su, Kaichun Mo, and Leonidas J Guibas. Pointnet: Deep learning on point sets for 3d classification and segmentation. In *Proceedings of the IEEE conference on computer vision and pattern recognition*, pages 652–660, 2017. [1](#)
- [31] Charles R Qi, Li Yi, Hao Su, and Leonidas J Guibas. Pointnet++: Deep hierarchical feature learning on point sets in a metric space. *arXiv preprint arXiv:1706.02413*, 2017. [1](#)
- [32] Daxuan Ren, Jianmin Zheng, Jianfei Cai, Jiatong Li, Haiyong Jiang, Zhongang Cai, Junzhe Zhang, Liang Pan, Mingyuan Zhang, Haiyu Zhao, et al. Csg-stump: A learning friendly csg-like representation for interpretable shape parsing. In *Proceedings of the IEEE/CVF International Conference on Computer Vision*, pages 12478–12487, 2021. [3](#)
- [33] Shunsuke Saito, Zeng Huang, Ryota Natsume, Shigeo Morishima, Angjoo Kanazawa, and Hao Li. Pifu: Pixel-aligned implicit function for high-resolution clothed human digitization. In *Proceedings of the IEEE/CVF International Conference on Computer Vision*, pages 2304–2314, 2019. [1](#), [2](#)
- [34] Mo Shan, Qiaojun Feng, You-Yi Jau, and Nikolay Atanasov. Ellipsdf: Joint object pose and shape optimization with a bi-level ellipsoid and signed distance function description. In *Proceedings of the IEEE/CVF International Conference on Computer Vision*, pages 5946–5955, 2021. [2](#)
- [35] Vincent Sitzmann, Julien Martel, Alexander Bergman, David Lindell, and Gordon Wetzstein. Implicit neural representations with periodic activation functions. *Advances in Neural Information Processing Systems*, 33, 2020. [3](#)
- [36] Matthew Tancik, Pratul P Srinivasan, Ben Mildenhall, Sara Fridovich-Keil, Nithin Raghavan, Utkarsh Singhal, Ravi Ramamoorthi, Jonathan T Barron, and Ren Ng. Fourier features let networks learn high frequency functions in low dimensional domains. *arXiv preprint arXiv:2006.10739*, 2020. [3](#)
- [37] Nanyang Wang, Yinda Zhang, Zhuwen Li, Yanwei Fu, Wei Liu, and Yu-Gang Jiang. Pixel2mesh: Generating 3d mesh models from single rgb images. In *Proceedings of the European Conference on Computer Vision (ECCV)*, pages 52–67, 2018. [1](#), [2](#), [5](#)
- [38] Jiajun Wu, Chengkai Zhang, Tianfan Xue, William T Freeman, and Joshua B Tenenbaum. Learning a probabilistic latent space of object shapes via 3d generative-adversarial modeling. *arXiv preprint arXiv:1610.07584*, 2016. [1](#)
- [39] Haozhe Xie, Hongxun Yao, Xiaoshuai Sun, Shangchen Zhou, and Shengping Zhang. Pix2vox: Context-aware 3d reconstruction from single and multi-view images. In *Proceedings of the IEEE/CVF International Conference on Computer Vision*, pages 2690–2698, 2019. [2](#)
- [40] Shun Yao, Fei Yang, Yongmei Cheng, and Mikhail G Mozerov. 3d shapes local geometry codes learning with sdf. In *Proceedings of the IEEE/CVF International Conference on Computer Vision*, pages 2110–2117, 2021. [3](#)
- [41] Kangxue Yin, Zhiqin Chen, Hui Huang, Daniel Cohen-Or, and Hao Zhang. Logan: Unpaired shape transform in latent overcomplete space. *ACM Transactions on Graphics (TOG)*, 38(6):1–13, 2019. [1](#)
- [42] Zerong Zheng, Tao Yu, Qionghai Dai, and Yebin Liu. Deep implicit templates for 3d shape representation. In *Proceedings of the IEEE/CVF Conference on Computer Vision and Pattern Recognition*, pages 1429–1439, 2021. [2](#)